2026 IEEE/SICE International Symposium on System Integration (SII)
January 11-14, 2026. Cancún, México

Coil Winding Simulation Incorporating Copper Wire Contact to Predict Manufacturing Defects

Masato Nagano, Hidefumi Wakamatsu, Yoshiharu Iwata, Hironori Suzuki, Takumi Nakaue, and Takahiro Tanaka

Abstract—**To improve motor efficiency, aligned winding is crucial as it increases the slot fill factor through orderly wire placement. However, defects such as wire bulging and overlapping can arise from variations in winding speed, tension, and wire diameter, often requiring trial-and-error adjustments. While finite element methods have been used to analyze local deformation, they are computationally expensive for simulating the full winding process. We propose a mass-spring model for efficient wire simulation and extend it to three dimensions by considering wire-to-wire contact. To further reduce simulation time, we reduce the number of particles in low-impact regions and enable full 3D simulation. This method allows accurate prediction of bulging and overlapping, contributing to both winding quality and production efficiency in motor manufacturing.**

I. Introduction

In recent years, global warming has become a social problem and there is a growing movement to reduce greenhouse gases and save energy. Motors are used in various aspects of the electromechanical industry and improving motor efficiency greatly contributes to energy savings and CO_2 reduction[1].

Improving motor efficiency requires the advancement of winding technologies that can fully exploit electromagnetic performance. Among these, "aligned winding," which arranges coils in an orderly manner, has attracted significant attention[2-5]. This technique enhances the slot fill factor and maximizes the contact area between the core and copper wires, thereby contributing to reductions in copper loss and magnetic flux leakage. To achieve aligned winding, it is essential that the wires are positioned precisely while maintaining appropriate contact with one another. However, in actual manufacturing environments, multiple parameters—such as winding speed, wire tension, and wire diameter—interact in complex ways. These interactions often lead to defects such as “bulging” or “overlapping”. These defects not only degrade the final quality of the winding, but also necessitate trial-and-error adjustments to the manufacturing process, directly reducing production efficiency. Therefore, simulating the winding process to reproduce and visualize the mechanisms that lead to such defects in advance is an extremely effective approach.

Masato Nagano, Hidefumi Wakamatsu, and Yoshiharu Iwata are with Dept. of Materials and Manufacturing Science, Graduate School of Eng., Osaka University, Yamadaoka 2-1, Suita, Osaka 565-0871, Japan (e-mail: {masato.nagano, wakamatu, iwata} @mapse.eng.osaka-u.ac.jp).

Hironori Suzuki, Takumi Nakaue and Takahiro Tanaka are with Component Production Engineering Center, Mitsubishi Electric Corporation, 8-1-1, Tsukaguchi-Honmachi, Amagasaki City, Hyogo 661-8661, Japan (email:{ suzuki.hironori@ap, nakaue.takumi@ea, tanaka.takahiro@dx } .mitsubishielectric.co.jp).

Previous studies have also conducted analytical investigations into winding behavior. For example, finite element method (FEM)-based approaches have been employed to elucidate the mechanisms behind local deformation of copper wires and the occurrence of bulging during the winding process[6,7]. However, FEM-based approaches involve high computational costs and are therefore not well suited for long-duration analyses that cover the entire winding process. To address this challenge, our research group has proposed a method that dynamically simulates the entire winding process while significantly reducing computational cost, by representing the wire as a discrete spring-mass model [8]. This approach enables dynamic tracking of the winding behavior in a two-dimensional plane and has demonstrated the capability to reproduce the degree of bulging that occurs in response to variations in process parameters such as core rotation speed and wire tension.

In this study, we further advance our previous two-dimensional model and propose a novel three-dimensional winding simulation method that accounts for wire-to-wire contact. This approach enables the prediction of not only bulging, but also wire overlapping—one of the critical issues in motor winding processes. The paper presents the theoretical framework and computational methodology of the proposed 3D winding simulation, along with numerical analysis results that demonstrate its effectiveness.

II. Overview of Winding Process and Simulation

A. Importance of Copper Wire Contact in Winding Process.

In this study, we focus on a winding method in which the core rotates with increasing angular velocity while the copper wire nozzle is translated in the axial direction. From the second turn onward, the wire is laid in direct contact with previously wound layers to form an aligned winding structure. In practical settings, however, winding is performed at high speeds, where the interaction between wire tension, nozzle feed rate, and core acceleration becomes highly complex. At such speeds, slight variations in contact force between adjacent wires can result in undesirable phenomena such as local bulging or overlapping, in which the wire fails to settle in the intended position. Fig.1 shows the schematic diagram of winding process.

A key challenge in simulating this process is its long duration: a complete winding includes dozens of turns, followed by reverse-layer stacking. Since the placement of each new copper wire depends on the full geometry of previously wound wire, it is essential to simulate the entire winding history. However, this leads to a sharp increase in computational costs. To address this, we propose a simulation

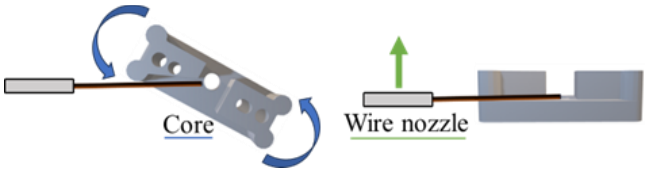

(a) Winding scheme (top view). (b) Winding scheme (side view).

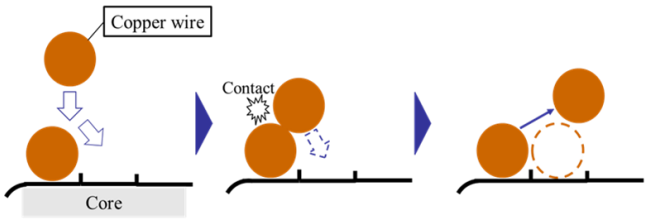

(c) A case where contact leads defects.

Figure 1. Schematic diagram of a winding process.

framework that models the copper wire as a spring-mass system with contact and friction forces, while also dynamically removing stationary mass points from the active computation. These excluded segments are converted into fixed cylindrical meshes that continue to interact with the wire being wound. This strategy enables accurate prediction of winding behavior—including the onset of overlap—while keeping computational demands tractable.

B. *Overview of simulation.*

In this study, following our previously proposed approach, the copper wire is discretely modeled using a spring-mass system, in which the wire is represented as a series of mass points connected by springs. A schematic illustration of this wire model is shown in Fig. 2. Each mass point is connected by straight springs, bending springs, and torsional springs. The forces acting on the mass points due to the straight and bending springs can be derived from the spatial coordinates $\boldsymbol{x}_i$ of the mass points. Torsional deformation is modeled by introducing a local coordinate system $\mathrm{P}_i - \xi_i\eta_i\zeta_i$ at each mass point and representing the rotational motion using quaternions $\boldsymbol{q}_i = [q_{0,i} \quad q_{1,i} \quad q_{2,i} \quad q_{3,i}]^{\mathrm{T}}$. It is important to note that a constraint that the ζ_i-axis is parallel to the straight spring must be satisfied even if the object coordinate system is rotated. The translational and rotational equations of motion for the i-th mass point are expressed as follows:

$$M\ddot{\boldsymbol{x}}_i = \boldsymbol{f}_i, \qquad \frac{2}{5}Mr^2 Q_i \ddot{\boldsymbol{q}}_i = \boldsymbol{\tau}_i, \tag{1}$$

$$Q_i = \begin{bmatrix} -q_{1,i} & q_{0,i} & q_{3,i} & -q_{2,i} \\ -q_{2,i} & -q_{3,i} & q_{0,i} & q_{1,i} \\ -q_{3,i} & q_{2,i} & -q_{1,i} & q_{0,i} \end{bmatrix}, \tag{2}$$

where M denotes the mass of the point, r its radius. $\boldsymbol{f}_i$ represents the forces from the straight springs and bending springs, and $\boldsymbol{\tau}_i$ represents the torque from the torsional springs connected to the mass point. The matrix Q_i in (1) is defined by (2). By solving these equations of motion together with the corresponding constraint equations, and applying numerical integration methods such as the Runge-Kutta scheme to the resulting accelerations $\ddot{\boldsymbol{x}}$ and $\ddot{\boldsymbol{q}}$, the dynamic behavior of the copper wire can be accurately predicted.

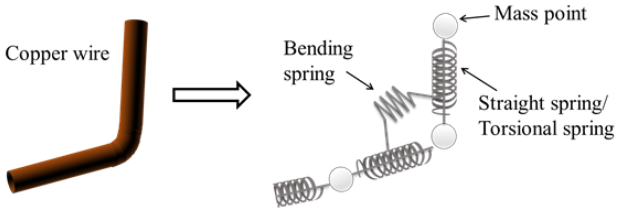

Figure 2. Model diagram of a copper wire.

III. MODELING OF CONTACT BETWEEN COPPER WIRE AND CORE

In the simulation of the winding process, it is essential to account for contact between the copper wire and the iron core. In this study, we formulate the contact interaction between the mass points of the wire and the surface of the iron core, which is discretized into triangular mesh elements.

We first determine whether a given mass point is located above a mesh element. Let the vertices of a triangle be denoted as $\boldsymbol{P}_{j-1}$, $\boldsymbol{P}_j$ and $\boldsymbol{P}_{j+1}$. Let $\boldsymbol{C}_k$ be the centroid of the triangle, which is given by

$$\boldsymbol{C}_k = \frac{\boldsymbol{P}_{j-1} + \boldsymbol{P}_j + \boldsymbol{P}_{j+1}}{3}. \tag{3}$$

The direction vectors of the edges of each triangular mesh $\boldsymbol{e}_j$ are defined such that they follow a counterclockwise order with respect to the outward normal vector of the mesh surface. Let $\boldsymbol{e}_j = \boldsymbol{P}_{j-1} - \boldsymbol{P}_j$ and define $\boldsymbol{a}_j = \boldsymbol{n}_k \times \boldsymbol{e}_j$, where $\boldsymbol{n}_k$ is the outward normal vector of the mesh surface. Under this convention, the centroid of the triangle is guaranteed to lie within the mesh, and consequently, $\boldsymbol{a}_j$ will point toward the interior of the triangle, as illustrated in Fig. 3(a). Therefore, if $(\boldsymbol{C}_k - \boldsymbol{P}_j) \cdot \boldsymbol{a}_j \geq 0$, it indicates that the edge direction vector is oriented clockwise with respect to the mesh normal vector. In this case, the vector $\boldsymbol{e}_j$ should be recalculated as $\boldsymbol{e}_j = \boldsymbol{P}_j - \boldsymbol{P}_{j+1}$ to ensure a consistent counterclockwise orientation.

Now, for a mass point $\boldsymbol{x}_i$, if it satisfies the following condition in (4) with respect to all triangle edges, it is determined to lie on or to the left of each edge, indicating that it is located above the mesh triangle.

$$\begin{aligned} (\boldsymbol{x}_i - \boldsymbol{P}_{j-1}) \cdot \boldsymbol{a}_{j-1} \geq 0 \cap (\boldsymbol{x}_i - \boldsymbol{P}_j) \cdot \boldsymbol{a}_j \geq 0 \\ \cap (\boldsymbol{x}_i - \boldsymbol{P}_{j+1}) \cdot \boldsymbol{a}_{j+1} \geq 0. \end{aligned} \tag{4}$$

Next, we evaluate whether the mass point—found to be above a given mesh—penetrates the mesh surface. In this study, contact is modeled using the penalty method[9]. When penetration occurs, a repulsive normal force is generated by a virtual spring placed on the mesh surface. The magnitude of the penetration $h_{i,k}$ is computed based on the distance vector $\boldsymbol{D}_{i,k}$ between the mass point and the triangle surface (Fig.3(b)). Distance vector $\boldsymbol{D}_{i,k}$ and penetration depth $h_{i,k}$ are defined as follows.

$$\boldsymbol{D}_{i,k} = \left\{(\boldsymbol{x}_i - \boldsymbol{P}_j) \cdot \frac{\boldsymbol{n}_k}{|\boldsymbol{n}_k|}\right\}\frac{\boldsymbol{n}_k}{|\boldsymbol{n}_k|}, \tag{5}$$

$$h_{i,k} = r - |\boldsymbol{D}_{i,k}| \geq 0. \tag{6}$$

The spring constant is denoted by k, the horizontal velocity component of the mass point relative to the mesh surface is

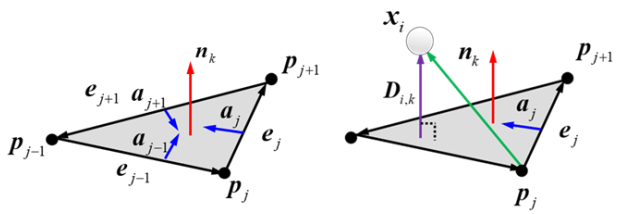

(a) $\boldsymbol{a}_j$ directed into the mesh. (b) Distance vector $\boldsymbol{D}_{i,k}$.

Figure 3. Schematic of vector relations between particle and mesh.

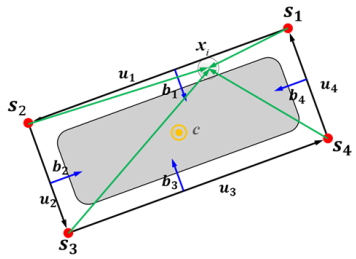

Figure 4. Schematic of region classification of a mass point.

donated by $\boldsymbol{v}_h$, and the coefficient of friction is donated by μ. Then, the equations of motion, with the addition of the normal force and frictional force, are given as follows:

$$M\ddot{\boldsymbol{x}}_i = \boldsymbol{f}_i + kh_{i,k}\boldsymbol{n}_k - \mu kh_{i,k}\frac{\boldsymbol{v}_h}{|\boldsymbol{v}_h|}. \tag{7}$$

By applying this procedure to all mass points and evaluating their contact with all mesh elements, a realistic simulation of the interaction between the copper wire and the iron core can be achieved.

IV. INTEGRATION OF STATIC COPPER WIRE WITH CORE

This section describes a method for excluding stationary mass points from the simulation after winding and integrating them into the iron core via mesh conversion. In dynamic simulations, computational cost is a critical concern. In our previously proposed method, a major challenge was the increasing number of mass points as the winding process progressed, which led to excessive computational load. The method proposed here addresses this issue by reducing the number of active mass points, thereby enabling long-duration simulations over multiple winding turns. The approach is explained in two parts: (*A*) a method for excluding stationary mass points from the calculation, and (*B*) a procedure for converting the excluded mass points into a mesh representation.

A. Excluding stationary mass points from the calculation.

The necessary condition for excluding stationary mass points from the simulation is considered here. To determine whether a mass point is stationary, its relative velocity with respect to the rotating iron core must be evaluated. Let $\boldsymbol{\omega}$ denote the angular velocity of the core, and $\boldsymbol{x}_c$ its center position. Then, the relative velocity $\boldsymbol{v}_r$ of the *i*-th mass point is given by follows:

$$\boldsymbol{v}_r = \dot{\boldsymbol{x}}_i - \boldsymbol{\omega} \times (\boldsymbol{x}_i - \boldsymbol{x}_c). \tag{8}$$

A mass point is regarded as stationary if the magnitude of $\boldsymbol{v}_r$ falls below a predefined threshold ($|\boldsymbol{v}_r| \cong 0$).

Next, to confirm that a mass point has completed the winding process, it is checked whether the point lies within a predefined region. The same algorithm used for determining whether a mass point is located above a mesh surface is adapted to evaluate whether the point lies within a designated region. To define this region, four points $\boldsymbol{s}_1, \boldsymbol{s}_2, \boldsymbol{s}_3, \boldsymbol{s}_4$ are positioned to enclose the iron core, and the direction vectors connecting these points in counterclockwise order are defined as $\boldsymbol{u}_1, \boldsymbol{u}_2, \boldsymbol{u}_3, \boldsymbol{u}_4$. Since the iron core rotates, these four points vary over time accordingly. Let $\boldsymbol{c}$ denote the central axis vector of the iron core. Then, the vector $\boldsymbol{b}$ is given by $\boldsymbol{b}_j = \boldsymbol{c} \times \boldsymbol{u}_j$ ($1 \leq \mathrm{j} \leq 4$), as illustrated in Fig.4. If the following condition in (9) is satisfied for all *j*, then the *i*-th mass point is considered to lie within the quadrilateral defined by $\boldsymbol{s}_1, \boldsymbol{s}_2, \boldsymbol{s}_3, \boldsymbol{s}_4$.

$$(\boldsymbol{x}_i - \boldsymbol{s}_j) \cdot \boldsymbol{b}_j \geq 0. \tag{9}$$

It should be noted that the margin around the outer perimeter of the iron core must be defined arbitrarily. If the margin is set to the radius of the mass point, bulging regions may not be excluded as intended. Therefore, as shown in Fig. 4, the margin is set to the diameter of the mass point to ensure proper exclusion of such deformations.

Mass points that satisfy both the stationary condition and the region condition described above are sequentially excluded from the simulation, starting from the fixed end of the wire. When the *n*-th (terminal) mass point is removed, the (*n*−1)-th mass point becomes the new terminal point. The endpoint constraint previously applied to the *n*-th point is transferred to the (*n*−1)-th point, with its parameters appropriately modified. In addition, the position of the removed mass point $\boldsymbol{x}_{out\_n}$ follows a rotational motion, as described below, and must be stored separately for subsequent mesh generation in the next step.

$$\boldsymbol{x}_{out\_n}(t) = \begin{bmatrix} \cos\{\theta_n(t)\} & 0 & sin\{\theta_n(t)\} \\ 0 & 1 & 0 \\ -sin\{\theta_n(t)\} & 0 & cos\{\theta_n(t)\} \end{bmatrix} \boldsymbol{x}_n, \tag{10}$$

$$\theta_n(t) = \omega_0(t - T_n) + \frac{1}{2}\alpha(t - T_n)^2. \tag{11}$$

Here, ω_0 denotes the initial angular velocity, and α represents the angular acceleration. T_n is the time at which the *n*-th mass point is excluded from the simulation.

By iteratively applying the above process in order from the terminal mass point, stationary mass points can be systematically excluded from the simulation.

B. Converting the excluded mass points into meshes.

The method for meshing the excluded mass points is now considered. Since the positions of the excluded mass points are known, a cylindrical mesh can be constructed based on these coordinates.

Consider the case in which the three consecutive mass points—*n*-th, (*n*−1)-th, and (*n*−2)-th—have been excluded from the simulation. To construct the cylindrical mesh, the central axis vectors $\boldsymbol{d}_i$ are defined as follows:

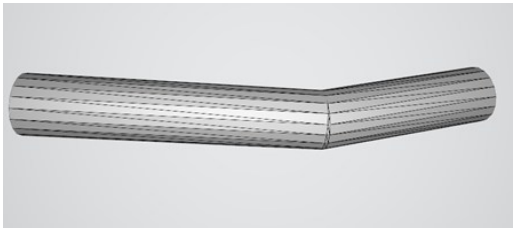

Figure 5. An example of cylindrical meshes.

$$\boldsymbol{d}_n = \boldsymbol{x}_n - \boldsymbol{x}_{n-1}, \qquad \boldsymbol{d}_{n-1} = \boldsymbol{x}_{n-1} - \boldsymbol{x}_{n-2}. \tag{12}$$

These vectors represent the local axial directions of the wire segments formed between the excluded mass points and serve as the basis for generating the cylindrical mesh geometry.

Next, to construct the circular cross-section of the cylinder, two orthonormal basis vectors perpendicular to the central axis are defined. As mentioned in Section II, Paragraph B, the ζ_i-axis in local coordinate systems is constrained to be parallel to the central axis $\boldsymbol{d}_i$, which ensures that the ξ_i- and η_i-axes are orthogonal to it. Therefore, by adopting these axes as the basis vectors, it becomes possible to generate a mesh that includes torsional information.

Using these basis vectors, the circular cross-section of the cylinder is constructed. The k-th vertex $\boldsymbol{V}_{n,k}$ on the circular cross-section centered at position $\boldsymbol{x}_n$ is given by follows:

$$\boldsymbol{V}_{n,k} = \boldsymbol{x}_n + r\cos\left(\frac{2\pi k}{N}\right)\boldsymbol{\xi}_n + r\sin\left(\frac{2\pi k}{N}\right)\boldsymbol{\eta}_n. \tag{13}$$

where N is the number of vertices used to approximate the circular cross-section, and $k = 0,1,\cdots,N$ -1. To ensure a smooth connection between consecutive cylindrical mesh segments, the circular cross-section centered at $\boldsymbol{x_{n-1}}$ is projected onto an intermediate plane that lies between the two adjacent axis vectors $\boldsymbol{d}_n$ and $\boldsymbol{d}_{n-1}$. This projection results in an elliptical cross-section as follows:

$$\begin{aligned}\boldsymbol{V}_{n-1,k} = \boldsymbol{x}_{n-1} + r\cos\left(\frac{2\pi k}{N}\right)\boldsymbol{\beta}_{n-1} \\ +r\left|\boldsymbol{d}_n \cdot \boldsymbol{d}_{avg}\right|\sin\left(\frac{2\pi k}{N}\right)\boldsymbol{\gamma}_{n-1},\end{aligned} \tag{14}$$

$$\boldsymbol{d}_{avg} = \frac{\boldsymbol{d}_n + \boldsymbol{d}_{n-1}}{|\boldsymbol{d}_n + \boldsymbol{d}_{n-1}|}\,. \tag{15}$$

A mesh is then constructed by connecting the point clouds of the circular and elliptical cross-sections generated as described above. Repeating this process for each pair of consecutive excluded mass points allows the entire meshed wire body to be reconstructed like an example in Fig. 5.

V. Simulation Results

Using the method described above, a 3D simulation of motor coil winding was conducted. The material properties used in the simulation are listed in Table 1. Material properties such as the coefficient of friction and spring stiffness were determined through a combination of property measurement experiments and simulations.

Fig. 6 shows an example of dynamic simulation results. One end of the copper wire is fixed at the center of core due to constraints, and as the winding progresses, mass points are sequentially excluded from the simulation, causing the constrained endpoint to shift accordingly. Fig. 7 presents the resulting 3D visualization. By translating the wire feed nozzle in the positive y-direction over time, a helical winding pattern is formed. In this simulation, the nozzle is moved with a pitch that prevents contact between adjacent turns of the wire.

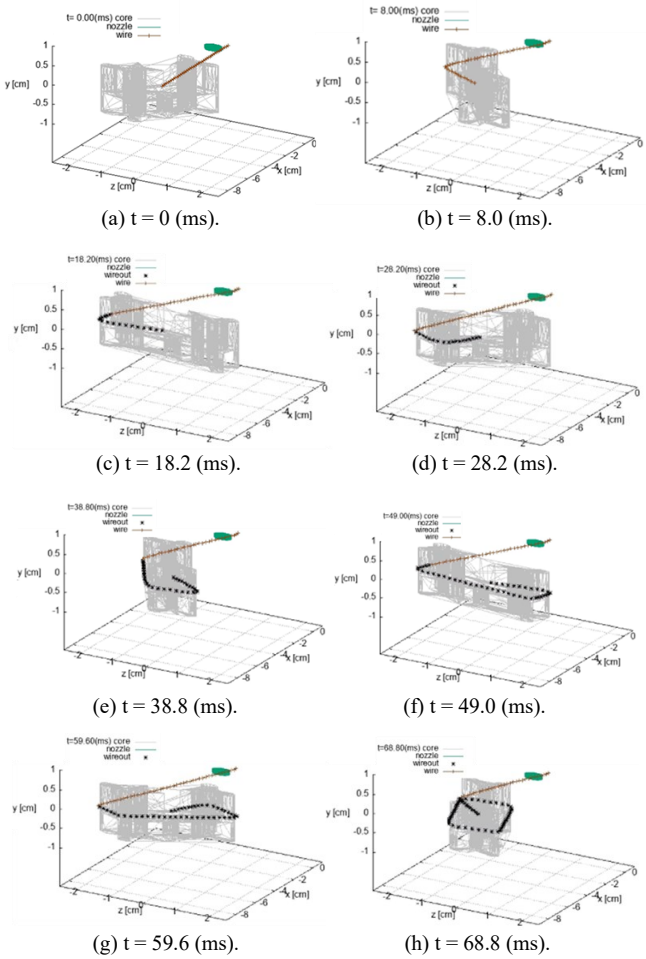

(a) t = 0 (ms). (b) t = 8.0 (ms). (c) t = 18.2 (ms). (d) t = 28.2 (ms). (e) t = 38.8 (ms). (f) t = 49.0 (ms). (g) t = 59.6 (ms). (h) t = 68.8 (ms).

Figure 6. An example of simulation results.

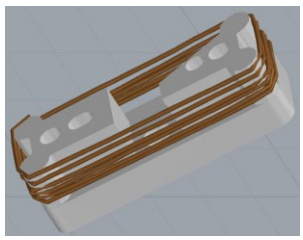

Figure 7. A results of 3D visualization.

Next, the pitch of the copper wire nozzle was adjusted so that the second winding turn comes into contact with the first-layer copper mesh at a distance equal to the wire radius. In typical motor winding processes, aligned winding is achieved by placing newly wound wires in contact with the previous layer and guiding them smoothly into adjacent positions.

To investigate the effect of winding speed on such contact, simulations were conducted at four different rotational

TABLE 1. PROPERTIES USED IN SIMULATION.

Copper wire diameter	ø 0.7 mm
Elongation rigidity in elastic deformation	4.89×10^4 N
Elongation rigidity in plastic deformation	1.10×10^3 N
Bending rigidity in elastic deformation	3.06×10^{-3} N $\cdot$ m^2
Bending rigidity in plastic deformation	1.13×10^{-4} N $\cdot$ m^2
Torsional rigidity in elastic deformation	4.32×10^{-3} N $\cdot$ m^2
Torsional rigidity in plastic deformation	9.0×10^{-5} N $\cdot$ m^2
Coefficient of static friction	0.23
Coefficient of kinetic friction	0.17

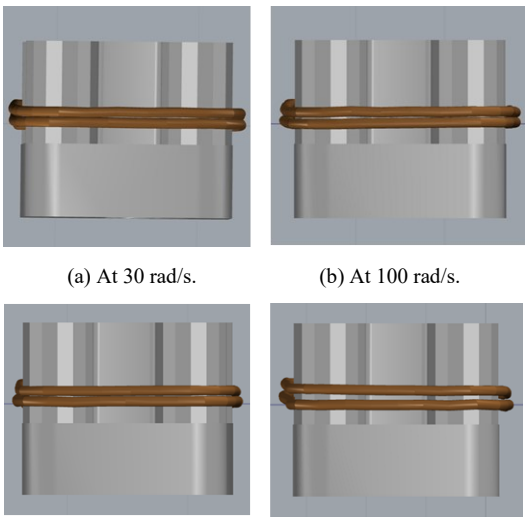

(a) At 30 rad/s. (b) At 100 rad/s.

(c) At 300 rad/s. (d) At 500 rad/s.

Figure 8. Comparison of winding conditions at different rotation speeds.

speeds: (a) 30 rad/s (≒286 rpm), (b) 100 rad/s (≒955 rpm), (c) 300 rad/s (≒2865 rpm) and (d) 500 rad/s (≒4775 rpm).

Fig. 8 shows the simulation results at the end of the second winding turn. In conditions (a) through (c), the wires remain in close contact after the second turn, maintaining an aligned winding pattern. However, in condition (d), a clear gap is observed between the first and second layers. This suggests that beyond a certain winding speed, the increased repulsive force during wire-to-wire contact disrupts the alignment, leading to gaps and a higher likelihood of overlap. Such disturbances are also observed in actual winding processes. The tendency for winding misalignment seen here qualitatively matches real-world behavior, providing supporting evidence for the validity of the proposed simulation method.

VI. CONCLUSION

In this study, a novel three-dimensional winding simulation method was proposed to reproduce the dynamic behavior of copper wire during motor coil winding, with special attention to wire-to-wire and wire-to-core contact phenomena. By extending our previous two-dimensional model to three dimensions and introducing a spring-mass representation with contact and friction modeling, the simulation enables prediction of defects such as bulging and wire overlap.

To address computational efficiency, a method for excluding stationary mass points from the simulation and converting them into a cylindrical mesh was introduced. This allows for long-duration simulations involving multiple turns, without excessive computational cost.

Simulation results demonstrated that winding quality is significantly affected by process parameters such as rotational speed. In particular, higher speeds led to increased repulsive forces during wire contact, resulting in winding misalignment—an observation consistent with real-world manufacturing trends.

In future work, the proposed method will be validated through experimental comparisons with actual winding machines, and the simulation outcomes will be leveraged to support and optimize real-world motor coil manufacturing processes. Furthermore, we will generalize this technique to other winding structures such as different slot shapes or multi-layer windings and explore its further application possibilities.

REFERENCES

[1] B.C. Mecrow, A.G. Jack, “Efficiency trends in electric machines and drives”, Energy Policy, Elsevier, vol. 36, No.12, 2008, pp.4336-4341

[2] H. Akita, Y. Nakahara, N. Miyake, T. Oikawa, “New Core Structure and Manufacturing Method”, IEEE 38th IAS Annual Meeting on Conference Record of the Industry Applications Conference, 2003

[3] T. Ishigami, “Arraying Winding Technology for Continuous Rectangular Wire Concentrated Wound Coils”, IEEJ Transactions on Industry Applications, Vol.138 No.8 pp.706-712

[4] J. Hagedorn, F. Sell-Le Blanc, J. Fleischer, “Handbook of Coil Winding”, Springer Vieweg Berlin, 2017, pp.139-224

[5] M. Masoumi, K. Rajasekhara, D. Parati, B. Bilgin, “Manufacturing Techniques for Electric Motor Coils With Round Copper Wires”, IEEE Access, Vol.10, 2022, pp.130212-130223

[6] F. Wirth, C. Nguyen, J. Hofmann, J. Fleischer, “Characterization of Rectangular Copper Wire Forming Properties and Derivation of Control Concepts for the Kinematic Bending of Hairpin Coils”, Procedia Manufacturing 47, 2020, pp.678-685

[7] M. Weigelt, A. Riedel, M. Masuch, A. Mahr, T. Glässel, J. Franke, “Potentials of an explicit finite element analysis of the bending processes for coated copper wires” 2017 7th International Electric Drives Production Conference (EDPC), 5-6 December, 2017

[8] M. Nagano, W. Hidefumi, I. Yoshiharu, S. Hironori, N. Takumi, T. Takahiro, “Dynamic Behavior analysis of Copper Wire for Motor Coil Manufacturing”, 2025 IEE/SICE International Symposium on System Integration (SII), 21-24 January, 2025.

[9] A.A. Shabana, “Dynamics of Multibody Systems”, Cambridge University Press (2013)